ECOHYDROLOGY
Ecohydrol. **7**, 427–439 (2014)
Published online 12 January 2013 in Wiley Online Library
(wileyonlinelibrary.com) DOI: 10.1002/eco.1362

An integrated modelling framework of catchment-scale ecohydrological processes: 1. Model description and tests over an energy-limited watershed

Guo-Yue Niu,[1]* Claudio Paniconi,[2] Peter A. Troch,[1,3] Russell L. Scott,[4] Matej Durcik,[1,5] Xubin Zeng,[1,6] Travis Huxman[1,7] and David C. Goodrich[4]

[1] *Biosphere 2 Earth Science, University of Arizona, USA*
[2] *Centre Eau, Terre et Environnement, Institut National de la Recherche Scientifique, Université du Québec, Quebec City, Canada*
[3] *Department of Hydrology and Water Resources, University of Arizona, USA*
[4] *Southwest Watershed Research Center, USDA-ARS, 2000 E. Allen Road, Tucson, AZ, 85719, USA*
[5] *SAHRA (Sustainability of semi-arid hydrology and riparian areas), University of Arizona, USA*
[6] *Department of Atmospheric Sciences, University of Arizona, USA*
[7] *Department of Ecology and Evolutionary Biology, University of Arizona, USA*

ABSTRACT

The interactions between atmospheric, hydrological, and ecological processes at various spatial and temporal scales are not fully represented in most ecohydrological models. This first of a two-part paper documents a fully integrated catchment-scale ecohydrological model consisting of a three-dimensional physically based hydrological model and a land surface model. This first part also presents a first application to test the model over an energy-limited catchment (8.4 km^2) of the Sleepers River watershed in Vermont.

The physically based hydrological model (CATchment HYdrology, CATHY) describes three-dimensional subsurface flow in variably saturated porous media and surface routing on hillslopes and in stream channels, whereas the land surface model (LSM), an augmented version of Noah LSM with multiple parameterization schemes (NoahMP), accounts for energy, water, and carbon flux exchanges between various land surface elements and the atmosphere. CATHY and NoahMP are coupled through exchanges of water fluxes and states. In the energy-limited catchment of the Sleepers River watershed, where snowmelt runoff generation is the dominant hydrologic flux, the coupled CATHY/NoahMP model at both 90 and 30-m surface grid resolutions, with minimal calibration, performs well in simulating the observed snow accumulation, and melt and subsequent snowmelt discharge. The Nash–Sutcliffe model efficiency of daily discharge is above 0.82 for both resolutions. The simulation at 90-m resolution shows a marginal improvement over that at 30-m resolution because of more elaborate calibration of model parameters. The coupled CATHY/NoahMP also shows a capability of simulating surface-inundated area and distributed surface water height, although the accuracy of these simulations needs further evaluation. The CATHY/NoahMP model is thus also a potentially useful research tool for predicting flash flood and lake dynamics under climatic change. Copyright © 2013 John Wiley & Sons, Ltd.

KEY WORDS coupling; physically-based hydrological model; land surface model; ecohydrological model; snowmelt runoff

Received 4 July 2012; Revised 15 November 2012; Accepted 30 November 2012

INTRODUCTION

Surface water in rivers, streams, lakes, and wetlands, subsurface water in the vadose zone and in shallow and deep aquifers, terrestrial ecosystems distributed over the landscape, and the atmospheric boundary layer are intimately coupled over a wide range of spatial and temporal scales. Accurate prediction of the response and feedback of atmospheric, hydrological, and ecological processes requires fully coupled numerical models describing the integrated ecohydrological response across a range of scales. Through lateral transport of water and solute, rainfall redistribution over catchments with complex terrain leads to unevenly distributed soil water, nutrient, and water stresses on plant growth, evapotranspiration, and soil carbon decomposition (Caylor *et al.*, 2004; Emanuel *et al.*, 2010; Riveros-Iregui *et al.*, 2011; Thompson *et al.*, 2011). A physically based ecohydrological model may help address key ecohydrological issues in water-limited environments, e.g. drought-induced tree die-off and invasion of nonnative shrubs over the southwest of the United States (Newman *et al.*, 2006). However, most of the current physically based models are inadequate to fully simulate these ecohydrological processes.

Most large-scale land surface models (LSMs) neglect the interactions between soil water and groundwater dynamics in the vertical direction, assuming a leaky soil bottom through gravitational drainage. It is only in the past decade that LSMs have started to include simple groundwater models, but they typically still do not explicitly account for lateral flows of surface water and groundwater (Liang *et al.*, 2003; Maxwell and Miller, 2005; Yeh and Eltahir, 2005; Niu *et al.*, 2007). Lateral flows of surface and subsurface water along hillslopes and streams, driven by topography, result in highly heterogeneous distributions of soil water at very small spatial scales (e.g. metres), affecting ecosystem productivity and diversity. It is thus important to accurately represent these flows in LSMs and ecohydrological models.

*Correspondence to: Guo-Yue Niu, Biosphere 2, P.O. Box 8746, Tucson, AZ 85738, USA. E-mail: niug@email.arizona.edu

Land surface models tend to operate at a higher resolution, for example, the North America Land Data Assimilation System at 1/8 degree (Xia *et al.*, 2012) and the Land Information System at 1-km resolution over the Continental United States (Peters-Lidard *et al.*, 2007). LSMs have accounted for subgrid soil moisture variations induced by subgrid variations in topography, soil properties, and vegetation type through various parameterization schemes (Entekhabi and Eagleson, 1989; Famiglietti and Wood, 1994; Liang *et al.*, 1994; Koster *et al.*, 2000; Seuffert *et al.*, 2002; Gedney and Cox, 2003; Niu *et al.*, 2005; Zeng *et al.*, 2008). However, these schemes, which were originally designed for continental-scale applications at a coarse resolution, may fail to represent nonlinear interactions between hydrological and ecological processes at smaller scales. For instance, the National Center for Atmospheric Research (NCAR) Community Land Model (CLM) (Oleson *et al.*, 2010) parameterizes the fraction of surface-saturated area and its effect on runoff production over large-grid cells (1×1 degree) using TOPMODEL concepts (Beven and Kirkby, 1979; Sivapalan *et al.*, 1987), but it neglects subgrid distributions of plants associated with subgrid distributions of soil moisture and their interactions.

Researchers have begun to pursue coupling LSMs with distributed hydrological models to fully represent the interactions between hydrological, ecological, and atmospheric processes at a higher spatial resolution (e.g. York *et al.*, 2002; Ivanov *et al.*, 2004; Rigon *et al.*, 2006; Yu *et al.*, 2006; Fan *et al.*, 2007; Miguez-Macho *et al.*, 2007; Kollet and Maxwell, 2008; Shen and Phanikumar, 2010; Xie *et al.*, 2012). The distributed hydrological models describe surface and subsurface flows at various levels of complexity, and they differ most significantly in descriptions of the subsurface, which is more computationally expensive. According to Kampf and Burges (2007), these integrated surface–subsurface models can be categorized into physically based models that solve the Richards equation (RE) (e.g. Kollet and Maxwell, 2006; Shen and Phanikumar, 2010, 2008) and simplified models that represent flow processes using analytical or other approximations (e.g. Ivanov *et al.*, 2004; Yu *et al.*, 2006). Physically based models solve either the three-dimensional (3D) RE for both unsaturated and saturated flows in a seamless manner (e.g. Kollet and Maxwell, 2006; Rigon *et al.*, 2006; Camporese *et al.*, 2010), or the one-dimensional (1D) RE for the unsaturated zone and a two-dimensional (2D) saturated flow model for groundwater (e.g. Shen and Phanikumar, 2010; Xie *et al.*, 2012) to save computational time. ParFlow coupled with a 2D kinematic wave surface flow model (Kollet and Maxwell, 2006) and CATHY (CATchment HYdrology model) coupled with a quasi-2D diffusive wave surface flow model (Camporese *et al.*, 2010) represent two of the most complex, physically based surface–subsurface flow models. These two models are different in many aspects such as spatial discretization, RE numerical solver, surface flow conceptualization, and coupling approach. Through a comparison of the two models, Sulis *et al.* (2010) showed that ParFlow and CATHY perform very similarly under most scenarios, with the most significant differences in discharge and saturation response occurring under scenario of infiltration excess and heterogeneous precipitation, due mainly to their different coupling approaches and spatial discretizations.

In this study, we couple the 3D, physically based CATHY surface–subsurface flow model with a widely used LSM, the NCAR community Noah model with multiple physics options representing atmospheric surface layer processes (NoahMP; Niu *et al.*, 2011). CATHY has undergone a long-term development in solving the 3D RE for variably saturated flow (Paniconi and Wood, 1993; Paniconi and Putti, 1994), solving the diffusive wave model for surface routing (Orlandini and Rosso, 1996, 1998), coupling the surface and subsurface flow models (Bixio *et al.*, 1999; Camporese *et al.*, 2010), and coupling a solute transport model to the flow model (Weill *et al.*, 2011). NoahMP augmented Noah's representations of momentum, energy, water, and carbon transfers within the vegetation canopy, snowpack, and soil and was coupled with the Weather Research and Forecast model for use in weather and short-term climate predictions. CATHY requires 'atmospheric forcing' fluxes (e.g. rainfall, snowmelt, transpiration, and soil-surface evaporation) as an upper boundary condition, a source term that can be effectively provided by NoahMP. Driven by energy (incoming shortwave and longwave radiation) and water (precipitation) inputs as well as other atmospheric states (wind, temperature, humidity, and pressure), NoahMP computes the surface atmospheric forcing fluxes over various land surfaces. NoahMP has its own representation of hydrology, which includes a solution of the 1D RE, a simple groundwater model, and a TOPMODEL-based runoff scheme. In the coupling, we replace NoahMP's hydrology with CATHY's 3D subsurface and quasi-2D surface diffusive wave flow model, resulting in an integrated ecohydrological model that links energy, water, and carbon processes for simulating catchment-scale hydrological and ecological dynamics under climate change. This complex, physically based ecohydrological model is a potentially powerful tool for understanding fundamental flow processes that control the interactions between hydrological and ecological processes.

In this first of a two-part paper, the major features of CATHY and NoahMP and of the coupling approach in space and time are described, and the coupled model is then applied to a humid catchment where snow accumulation and melt is a dominant runoff generation process. We also present simulation results from the 1D NoahMP model as a reference for assessing the coupled 3D model. In the second paper, we present a detailed application over a water-limited catchment in Arizona (7.92 ha) and discuss the important role of re-infiltration of overland flow on redistributions of soil moisture and on plant growth in semi-arid climates. The integrated CATHY/NoahMP model ultimately provides a basis for future coupling to other process models (e.g. reactive transport and soil erosion models) for the study of critical zone processes at hillslope scales (Huxman *et al.*, 2009) and for assessing the impacts of climate change on catchment-scale ecohydrological processes.

MODEL DESCRIPTION

We describe the main features of the CATHY and NoahMP models in this section. More detailed descriptions can be found in the work of Camporese *et al.* (2010) for CATHY and in the work of Niu *et al.* (2011) for NoahMP.

CATHY

CATHY is a coupled model system of subsurface and surface water flow at the catchment scale. The subsurface flow model solves the 3D RE describing flow in variably saturated porous media (Paniconi and Wood, 1993; Paniconi and Putti, 1994), i.e.

$$S_w S_s \frac{\partial \psi}{\partial t} + \phi \frac{\partial S_w}{\partial t} = \vec{\nabla}.\left[K_s K_r(\psi)\left(\vec{\nabla}\psi + \vec{\eta_z}\right)\right] + q_{ss} - q_{root} \quad (1)$$

where $S_w = \theta/\phi$ is relative soil saturation, θ is the volumetric moisture content ($m^3\,m^{-3}$), ϕ is the porosity ($m^3\,m^{-3}$), S_s is the aquifer specific storage coefficient (m^{-1}), ψ is pressure head (m), t is time (s), $\vec{\nabla}$ is the gradient operator (m^{-1}), K_s is the saturated hydraulic conductivity tensor ($m\,s^{-1}$), $K_r(\psi)$ is the relative hydraulic conductivity function (dimensionless), $\dot{\eta}_z = (0, 0, 1)$ is a unit vector representing vertical flows, z is the vertical coordinate directed upward (m), and q_{ss} and q_{root} represent distributed source (positive) or sink (negative), and root uptake of water (see section on Coupling of CATHY and NoahMP Processes) ($m^3\,m^{-3}\,s^{-1}$), respectively. Equation (1) is solved numerically with Galerkin finite elements in space using tetrahedral elements and linear basis functions, and with a weighted finite difference scheme for integration in time. It has three options for the nonlinear characteristic relationships of $K_r(\psi)$ and $S_w(\psi)$, i.e. van Genuchten and Nielsen (1985), Brooks and Corey (1964), or Huyakorn *et al.* (1984) formulations. It has two options for the linearized solver, i.e. Newton or Picard iteration. More details on the numerical aspects and other features of the subsurface solver can be found in the work of Paniconi and Putti (1994).

The upper boundary condition for Equation (1) is the atmospheric forcing in case of a Neumann boundary condition (specified flux):

$$-K_s K_r(\psi)\left.\frac{\partial(\psi + z)}{\partial z}\right|_{z=z_{surf}} = q_{in} \quad (2)$$

where q_{in} ($m\,s^{-1}$) is the water flux incident at the soil surface, z_{surf}. The upper boundary condition can be switched into a Dirichlet condition (specified pressure head) depending on the saturation state of a given node, i.e. whether the node is currently ponded, saturated, below saturation, or air-dry (see details by Camporese *et al.*, 2010).

The surface flow model solves the diffusion wave equation describing surface flow propagation over hillslopes and in stream channels identified using terrain topography and the hydraulic geometry concept (Orlandini and Rosso, 1996, 1998), i.e.

$$\frac{\partial Q}{\partial t} + c_k \frac{\partial Q}{\partial s} = D_h \frac{\partial^2 Q}{\partial s^2} + C_k q_s \quad (3)$$

where s is the 1D coordinate system (m) describing each element of the drainage network, Q is the discharge along the rivulet/stream channel ($m^3\,s^{-1}$), c_k is the kinematic celerity ($m\,s^{-1}$), D_h is the hydraulic diffusivity ($m^2\,s^{-1}$), and q_s is the inflow (positive) or outflow (negative) rate from the subsurface to the surface ($m^3\,m^{-1}\,s^{-1}$). The model accounts for two surface routing processes, i.e. hillslope (overland) flow in rills and rivulets, and stream flow in channels. It also accounts for surface water storage in streams, pools, and lakes and their retardation effects on surface flow. It is coupled with the subsurface flow model through infiltration/exfiltration in/from subsurface soils, i.e. q_{ss} and q_s in Equations (1) and (3).

The drainage network that defines the upstream drainage areas for each grid cell and the flow directions along the rill and channel networks are derived from analysis of digital elevation model (DEM) data performed as a pre-processing step. The pre-processor provides three options for schemes to derive flow directions, i.e. classical D8 single-direction (Marks *et al.*, 1984; O'Callaghan and Mark, 1984), D∞ multiple-direction (Tarboton, 1997), and D8-LTD single-direction (Orlandini and Moretti, 2009a, 2009b). It involves three operations: (i) arranging all the DEM cells of the catchment in a descending order according to their elevation values; (ii) recursively raising the elevations of the cells located in flat or depressed areas to ensure a drainage direction with a small positive slope for all the cells of the catchment; and (ii) rearranging the DEM cells in a descending order. The pre-processor also identifies lakes and other significant topographic depressions through a 'lake boundary-following' procedure (Mackay and Band, 1998) that forces the water around the lake boundary to form a circulation, draining to the lake outlet.

The advection-diffusion Equation (3) is solved with the Muskingum-Cunge method for both hillslope rill and channel network flows, with different hydraulic geometry parameters describing the characteristics of these two flow regimes (Orlandini and Rosso, 1998; Orlandini, 2002; Camporese *et al.*, 2010). The model routes surface runoff downstream from the uppermost DEM cell in the basin to the outlet, following the drainage network determined by the pre-processor. A given grid cell receives water from its upslope neighbours and discharges water to one (in the case of the D8 and D8-LTD single-direction algorithms) or two (in the case of the D∞ multiple-direction algorithm) downslope neighbours. It also receives or releases water internally from/to the subsurface, through the q_{ss} and q_s terms in Equations (1) and (3) (rendered dimensionally consistent through appropriate use of cell area and network length factors).

NoahMP

NoahMP is an augmented version of the Noah LSM for operational use in weather forecast and short-term climate prediction (Chen and Dudhia, 2001; Ek *et al.*, 2003). NoahMP significantly augments the physical realism of the Noah LSM through a community effort (Niu *et al.*, 2011). NoahMP accounts for surface energy, water, and carbon fluxes over soil, snow, and vegetation surfaces. The

improvements include adding the following: (i) a vegetation canopy layer to distinguish the canopy temperature from the ground temperature; (ii) a modified two-stream approximation of radiation transfer that accounts for the effects of 3D canopy structure on beam and diffusive radiation over visible and near-infrared wave bands (Niu and Yang, 2004); (iii) a 3-layer, process-based snow model to accommodate snowpack internal physical processes, e.g. retention and refreezing of liquid water (Yang and Niu, 2003); (iv) a frozen soil scheme that separates permeable and impermeable fractional areas (Niu and Yang, 2006); (v) a simple groundwater model with a TOPMODEL-based runoff scheme (Niu *et al.*, 2007); and (vi) a short-term dynamic vegetation model (Dickinson *et al.*, 1998).

NoahMP has a structure of one canopy layer, three snow layers, and four soil layers. It computes surface temperature by iteratively solving the surface energy balance of solar radiation, longwave radiation, sensible heat, latent heat, and ground heat fluxes. It uses a 'semi-tile' method to deal with surface heterogeneity. The advantage of the 'semi-tile' method over the traditional 'tile' method is to avoid overlapping of shadows on the ground or understory canopies. NoahMP represents photosynthesis of C3 plants following the model of Farquhar *et al.* (1980) modified by Collatz *et al.* (1991), whereas that of C4 plants following Collatz *et al.* (1992). The rate of gross photosynthesis is computed as the minimum of three limiting factors: Rubisco limitation, light limitation, and that associated with transport of photosynthetic products for C3 plants and PEP-carboxylase limitation for C4 plants. It also includes a short-term vegetation phenology model that describes allocation of the assimilated carbon to carbon storages in various parts of the plant (leaf, stem, wood, and root), death due to cold and drought stresses, and turnover due to senescence, herbivory, or mechanical loss (Dickinson *et al.*, 1998). Leaf area index (LAI) is converted from the leaf carbon storage through specific leaf area ($m^2\,g^{-1}C$), which is dependent on vegetation types. NoahMP assumes uniformly distributed roots in the vertical direction and varying root depth depending on vegetation type.

NoahMP also has its own hydrological schemes. It solves the 1D RE within four soil layers with thicknesses of 0.1, 0.3, 0.6, and 1.0 m. Both surface runoff and subsurface runoff (or baseflow) are parameterized as exponential functions of the water table depth (Niu *et al.*, 2005) following TOPMODEL concepts (Beven and Kirkby, 1979; Sivapalan *et al.*, 1987). The water table depth is solved through a simple groundwater model, a modified version of Niu *et al.* (2007). It also keeps the original runoff scheme (Schaake *et al.*, 1996), which describes mainly infiltration-excess runoff and is considered more effective in semi-arid regions (Niu *et al.*, 2012), as an option.

NoahMP also provides multiple options of schemes to represent a wide range of physical processes including radiation transfer through the vegetation canopy, stomatal conductance, drought stress factor for stomatal conductance, aerodynamic resistance, and snow and frozen soil. It thus provides a framework to compare different parameterization schemes within the same model.

Coupling of CATHY and NoahMP processes

In the coupled model of CATHY and NoahMP, the hydrological schemes of NoahMP including the 1D soil moisture solver, the TOPMODEL-based runoff scheme, and the simple groundwater model were removed. The two models are then coupled by exchanging their state variables, i.e. liquid soil water and water fluxes. Land surface energy exchanges with the atmosphere, described by NoahMP, are not exchanged with CATHY. CATHY transfers its soil moisture to NoahMP, and NoahMP, in turn, transfers water fluxes including q_{in} and q_{root} to CATHY (Figure 1). NoahMP accounts for melting or refreezing of soil water by assessing the energy excess or deficit relative to freezing point, which is variable below 273.16 K and is represented with the freezing-point depression equation (see details in the work of Niu and Yang, 2006), and transfers the resulting soil liquid water back to CATHY.

Water flux incident on soil surface, q_{in}. The atmospheric forcing term, q_{in} (m s^{-1}), is the residual of water incident on the soil surface minus surface evaporation:

$$q_{\text{in}} = q_{\text{drip}} + q_{\text{through}} + q_{\text{bot}} - q_{\text{eva}} \tag{4}$$

where q_{drip}, q_{through}, q_{bot}, and q_{eva} are rates (m s^{-1}) of drip from the vegetation canopy-intercepted water, throughfall, snowmelt water flowing out of the bottom of the snowpack, and soil-surface evaporation (or dew) computed by NoahMP. The drip rate of liquid water from the vegetation canopy is

$$q_{\text{drip}} = F_{\text{veg}}P_{\text{r}} - \min\left(F_{\text{veg}}P_{\text{r}}, \frac{C_{\text{l,max}} - C_{\text{l}}}{\Delta t}\left(1 - e^{-\frac{P_{\text{r}}\Delta t}{C_{\text{l,max}}}}\right)\right) \tag{5}$$

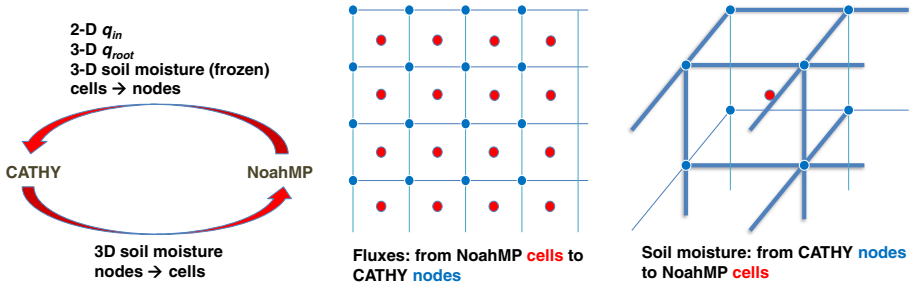

Figure 1. Schematic diagram showing the coupling of CATHY with NoahMP.

where the first term at the right-hand side represents rain (P_r) falling on the vegetation canopy and the second term represents the interception capability for liquid water. F_{veg} is the vegetation cover fraction predicted by the dynamic vegetation model (see Niu *et al*., 2011 for details). C_l and $C_{l,max}$ are canopy-intercepted liquid water and its maximum value, respectively, depending on the predicted LAI. Δt is the NoahMP timestep. NoahMP also considers interception of snowfall by the canopy, refreeze of liquid water, and melt of ice on the canopy, which affects C_l and thus the drip rate (Niu and Yang, 2004). The throughfall rate is the rainfall that is not intercepted by the canopy:

$$q_{through} = \left(1 - F_{veg}\right)P_r \tag{6}$$

In case of a snow-covered surface, q_{drip} and $q_{through}$ fall on the snow surface and exchange energy with the snowpack, with a portion of these fluxes flowing out of the bottom of the snowpack (q_{bot}) and the rest being held, frozen, and retained in the snowpack depending on the thermal state of the snowpack. The surface evaporation rate q_{evap} is an average of evaporation from the bare-soil surface ($q_{e,b}$) and from the soil surface underneath the vegetation canopy ($q_{e,v}$), weighted by F_{veg}:

$$q_{eva} = \left(1 - F_{veg}\right)q_{e,b} + F_{veg}q_{e,v} \tag{7}$$

$q_{e,b}$ and $q_{e,v}$ are parameterized according to Monin–Obukhov similarity theory:

$$q_{e,b} = \frac{\rho C_p}{\gamma L_v}\ \frac{e_{sat}\left(T_{g,b}\right)h_g - e_{air}}{r_{aw} + r_{soil}} \tag{8a}$$

$$q_{e,v} = \frac{pC_p}{\gamma L_v}\ \frac{e_{sat}\left(T_{g,v}\right)h_g - e_{ac}}{r_{aw,g} + r_{soil}} \tag{8b}$$

where ρ is air density (kg m^{-3}), C_p is dry-air specific heat capacity (=1005 J kg^{-1} K^{-1}), L_v is the latent heat of vaporization (J kg^{-1}), and γ is the psychrometric constant (Pa K^{-1}). e_{air} and e_{ac} are the water vapour pressures (Pa) of the atmosphere at a reference height, z_{ref} (or the measurement height; m) and of the canopy air, respectively. $e_{sat}(T_{g,b})$ is the saturated water vapour pressure (Pa) at the temperature of the bare-soil surface ($T_{g,b}$) and $e_{sat}(T_{g,v})$ is the saturated water vapour pressure (Pa) at the temperature of the vegetated soil surface ($T_{g,v}$). r_{aw} (s m^{-1}) is the aerodynamic resistance between soil-surface roughness length, $z_{0,g}$, and z_{ref}, $r_{aw,g}$ is the aerodynamic resistance for water vapour below the canopy (between $z_{0,g}$ and $d_0 + z_{0,c}$, where d_0 and $z_{0,c}$ are the zero-displacement height in m and roughness length of the canopy, respectively) with a correction for atmospheric stability (Niu and Yang, 2004), and r_{soil} (s m^{-1}) is the soil-surface resistance accounting for the resistance on water vapour transfer from the surface soil pore space to the roughness length for heat (z_{0h}) using an empirical formulation of Sellers *et al*. (1992). h_g is the relative humidity of the air in the surface soil pore space (relative to the saturated vapour pressure at the water surface attached to soil particles).

As represented in NoahMP, a portion of liquid water (resulting from snowmelt or rain falling on the snow surface) in a snow layer is held in that layer while any residual flows down to its lower neighbour layer. q_{bot} is the liquid water that cannot be held by the bottom layer, flowing out of the bottom of the snowpack. Melting of ice or refreezing of liquid water held in a layer, $q_{m,i}$, is assessed through the energy excess or deficit needed to change a snow layer temperature to the freezing point, T_{frz}:

$$q_{m,i} = C_i \Delta z_i \frac{T_i - T_{frz}}{\Delta t L_f} \tag{9}$$

where L_f is the latent heat of fusion (=0.3336 $\times$ 10^6 J kg^{-1}) and T_i and Δz_i are the temperature and snow layer thickness of the ith layer. C_i is the volumetric heat capacity of the ith snow layer:

$$C_i = C_{ice}\theta_{ice,i} + C_{liq}\theta_{liq,i} \tag{10}$$

where $\theta_{ice,i}$ and $\theta_{liq,i}$ are the partial volume of ice and liquid water of the ith snow layer and C_{ice} (2.094 $\times$ 10^6 J m^{-3} K^{-1}) and C_{liq} (4.188 $\times$ 10^6 J m^{-3} K^{-1}) are the volumetric heat capacity for ice and liquid water, respectively.

Root uptake of water, q_{root}. Root water uptake and subsequent transpiration, q_{root} (m s^{-1}), occurs only through a fraction of leaves that are not covered by water, $1 - f_{wet}$, where f_{wet} is the wet fraction of the canopy, and it is controlled by the water vapour gradient between leaf cavity ($e_{sat}(T_v)$) and surrounding air (e_{ac}):

$$q_{root} = \frac{\rho C_p}{\gamma L_v}(1 - f_{wet})\left(\frac{L_{e,sun}}{r_b + r_{s,sun}} + \frac{L_{e,sha}}{r_b + r_{s,sha}}\right)\left(e_{sat}(T_v) - e_{ac}\right) \tag{11}$$

where f_{wet} takes the form suggested by Deardorff (1978). $L_{e,sun}$ and $L_{e,shd}$ are effective sunlit and shaded LAI, respectively. $r_{s,sha}$ and $r_{s,sun}$ are stomatal resistances per unit LAI for shaded leaves and sunlit leaves, respectively. The shaded and sunlit fractions of leaves are computed through a two-stream radiation transfer scheme (Dickinson, 1983). r_b is leaf boundary layer resistance per unit LAI following Brutsaert (1982), and $e_{sat}(T_v)$ is the saturated water vapour pressure (Pa) at the canopy temperature T_v.

The transpiration q_{root} is then distributed to soil layers, $q_{root,i}$ (m^3 m^{-3} s^{-1}), proportional to root fractions (or layer thickness in the case of evenly distributed roots) and the state of soil moisture of the layers, as

$$q_{root,i} = \frac{A_{node}}{V_{node}}\left(\frac{\Delta z_i}{z_{root}}\beta_i \Big/ \sum_{j=1}^{N_{root}} \frac{\Delta z_j}{z_{root}}\beta_j\right) q_{root} \tag{12}$$

where Δz_i is the soil layer thickness, N_{root} is the total number of soil layers containing roots, z_{root} is the total depth of the root zone, β_i is the soil moisture factor (or drought stress factor), and A_{node} and V_{node} are the area and volume associated to a given CATHY node. NoahMP provides three optional schemes for the β_i factor. The current model version does not include root dynamics, and thus, z_{root} is prescribed

through a lookup table of NoahMP. Also note that Δz_i is determined through CATHY modules and transferred to NoahMP.

Formulations of the related surface energy fluxes, e.g. net radiation received by the vegetation canopy and the ground, sensible and latent heat fluxes, and ground heat fluxes, are described in detail in the work of Niu *et al.* (2011).

Spatial conversion. CATchment HYdrology solves soil moisture at grid nodes, i.e. the intersection points, whereas NoahMP computes q_{in} and q_{root} at grid cells covering the grid area (Figure 1). To couple the two models, CATHY needs to transfer its nodal soil moisture values to NoahMP and NoahMP, in turn, needs to transfer its q_{in} and q_{root} water fluxes over the grid boxes, as well as its update of liquid soil water in the case of frozen soil, to CATHY. For an inner CATHY node (blue dots in Figure 1), surface fluxes such as q_{in} are computed as the arithmetic average of the four surrounding NoahMP grid cells. For a corner node, the flux is simply that of the closest NoahMP grid cell. For a border node, it is computed as the average of the values at the two closest NoahMP cells. The same logic is applied to subsurface variables such as q_{root} and liquid soil water, with the averaging in this case performed over a maximum of eight NoahMP cells adjoining a given CATHY node. In the other direction, soil moisture at a NoahMP cell (red dot) is computed as the arithmetic average of the values from its eight surrounding CATHY nodes (blue dots).

Time scheme. CATHY fast hydrological processes were coupled with the relatively slower land surface energy and ecological processes by combining multiple time scales. Time stepping in CATHY is adapted to the convergence behaviour of the subsurface solver and includes a further level of nested time scales, allowing smaller time steps to be taken for the surface routing scheme within each step of the subsurface solver (see Camporese *et al.* (2010) for details). NoahMP computes land surface processes, such as surface energy and water fluxes, photosynthesis, respiration, and stomatal resistance at a fixed time step (e.g. 1800 s), which is determined by the frequency of atmospheric forcing data. In the coupled model, the shorter, varying time step of CATHY (e.g. less than 900 s and down to 0.1 s) is further adapted to match NoahMP time steps whenever a CATHY time step passes the end of a NoahMP step.

MODEL TESTING

We tested the coupled CATHY/NoahMP model over a subcatchment of the Sleepers River, Vermont. The Sleepers River dataset has been selected by the World Meteorological Organization as one of six high quality datasets for its project on the Intercomparison of Models of Snowmelt Runoff. To test the coupled model's ability to simulate streamflow, we used the observational dataset from subcatchment W3 (8.4 km^2; 44.43°N, 72.42°W) of the Sleepers River watershed (111 km^2) located in the highlands of Vermont, USA. The dataset provides atmospheric forcing, snow properties, and streamflow data from 1969 to 1974 at hourly intervals. The atmospheric forcing data include incoming shortwave radiation, downward longwave radiation, precipitation, 2-m air temperature and humidity, wind speed, and air pressure. The W3 topography is characterized by rolling hills, and the soils are dominated by silty loams. The local vegetation is approximately one-third grassland, one-third coniferous forest, and one-third deciduous forest. Additional details about the Sleepers River watershed dataset are provided by Lynch-Stieglitz (1994). The DEM data were downloaded from the Advanced Spaceborne Thermal Emission and Reflection Radiometer 30-m resolution Global Digital Elevation Model in Geo TIFF format (http://asterweb.jpl.nasa.gov/gdem.asp).

We ran the coupled model at two grid resolutions, 30 and 90 m, from November 1969 to November 1974 to investigate the model's ability to simulate discharge, surface-saturated area, and surface water depth at different resolutions. For the coupled model, the timestep for NoahMP is 3600 s and for CATHY is a maximum of 1200 s. The river networks at 30 and 90-m resolution are derived from the 30-m DEM and the aggregated 90-m DEM, respectively, using CATHY's pre-processor (Figure 2).

We also ran the original 1D NoahMP model (i.e. with its own hydrological schemes) in standalone mode, comparing it to the coupled model to assess any improvements obtained with CATHY/NoahMP. The standard NoahMP has four soil layers with thicknesses of 0.1, 0.3, 0.6, and 1.0 m. NoahMP has three options for runoff schemes, and Niu *et al.* (2011) demonstrated that the TOPMODEL-based runoff scheme is superior to the other schemes for this energy-limited catchment. The TOPMODEL-based scheme requires the water table depth to compute both surface and subsurface

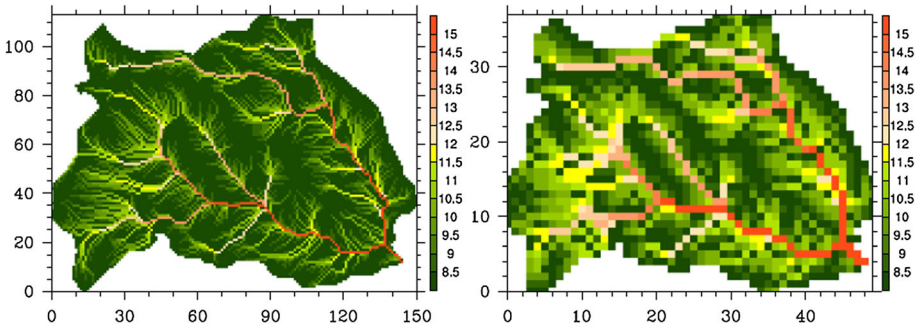

Figure 2. The upstream area, a, scaled by natural logarithm, $\ln(a)$ of the W3 subcatchment of the Sleepers River watershed, Vermont at 30 m (left) and 90 m (right) resolutions.

runoff. We use a simple groundwater model (Niu *et al.*, 2007) to compute recharge rate to the groundwater, which is actually the NoahMP's lower boundary (at 2.0 m). The recharge rate can be downward or upward depending on the gradient between the water head at the bottom soil layer and that at the water table (see Niu *et al.*, 2011 for further details). The TOPMODEL-based runoff scheme uses the same maximum saturated fraction ($F_{max} = 0.42$) and mean value of topographic index ($\lambda_m = 7.26$) as used in the work of Niu *et al.* (2005).

The coupled CATHY/NoahMP model was set up with five soil layers with thicknesses of 0.1, 0.3, 0.6, 1.0, and 2.0 m. The thicknesses of the top four layers were set up exactly as those of the 1D NoahMP model, whereas the fifth (bottom) layer was added to contain the water table in the model domain. The lower boundary (4.0 m) was then sealed with a zero-flux boundary condition. This is a reasonable setup for a fair comparison with the 1D NoahMP model, whose lower boundary condition at 2.0 m is the recharge rate provided by the simple groundwater model of Niu *et al.* (2007). The lateral boundaries of the coupled CATHY/NoahMP are sealed with zero-flux boundary conditions.

We selected the same Noah-type drought stress factor for both the CATHY/NoahMP and NoahMP models out of three options. Both the coupled CATHY/NoahMP and 1D NoahMP models used the same soil (silty loam) and vegetation (grass) parameters based on the lookup tables associated with NoahMP. The 1D NoahMP model selected grassland as the dominant vegetation type to represent the entire catchment, mainly because the snow property observations were from a grassland site. To be consistent, the spatially distributed CATHY/NoahMP used the same vegetation type. In addition, spatially distributed vegetation data at such a high resolution (30 m) were not available during the modelling period (1969–1974). How spatially varying vegetation type (grassland versus forest) affects the total amount of discharge through its impact on evapotranspiration is worth investigating in future studies.

We optimized the hydraulic conductivity decay factor in the TOPMODEL-based runoff scheme, which greatly affects both recessions and peaks of discharge, in the 1D NoahMP simulation. For the CATHY/NoahMP model, we calibrated the saturated hydraulic conductivity K_s and the van Genuchten and Nielsen (1985) fitting parameter n against the observed discharge at 90-m resolution and then applied it to the 30-m resolution (to save computational time). The optimized K_s and n values for the 90-m simulations are 2.0×10^{-4} m s^{-1} and 1.26, respectively. Both the 30 and 90-m simulations were initialized with equilibrium states that resulted from 5-year (1969–1974) model spin-up runs at the respective 30 and 90-m resolutions.

For the 30-m resolution simulation, we fixed CATHY's iteration number for the subsurface solver to three regardless of convergence to reduce computational time. To complete a 175-day simulation at 30-m resolution, CATHY/NoahMP with 15 maximum iterations and a backstepping scheme (to handle convergence failures) took 16 times as much CPU as the fixed three-iteration run. We first compared the results of the fixed three-iteration run to the 15-iteration run at 90-m resolution and found that the differences between the two simulations for runoff and surface-saturated area were 0.9% and 0.6%, respectively. These small differences may justify using the three-iteration limit for this energy-limited catchment, but for the water-limited catchment (see the companion paper), the fixed three-iteration was found to produce significant errors and thus was not used.

RESULTS

Both the coupled CATHY/NoahMP and 1D NoahMP models simulated snow water equivalent (SWE) and snow depth very well for both snow accumulation and ablation periods (Figure 3). CATHY/NoahMP produced almost the same catchment-averaged snow properties and q_{in} as did 1D NoahMP, because both models used the same snow-related parameters, e.g. snow surface albedo and roughness length. The current version of the coupled model

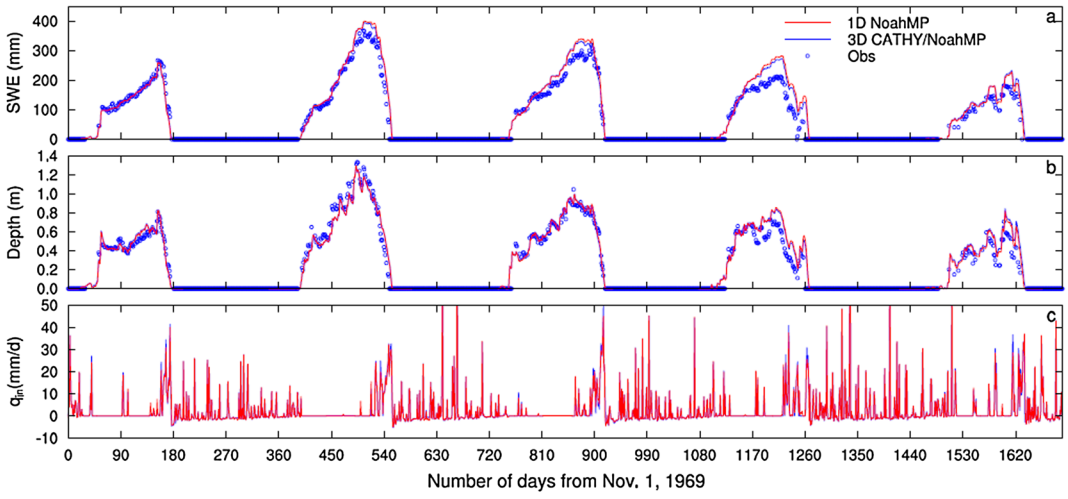

Figure 3. Daily mean (a) snow water equivalent (SWE) (mm), (b) snow depth (m), and (c) q_{in} (mm d^{-1}) averaged over the W3 subcatchment of the Sleepers River watershed, Vermont. The results from the two simulations nearly overlap.

does not predict temperature of surface and subsurface water flows, and the effects of terrain slope and aspect on absorption of solar radiation. For these reasons, the coupled CATHY/NoahMP model produces SWE and snow depth very similar to 1D NoahMP. In Figure 3(c), q_{in} produced by NoahMP as an input to CATHY contains positive values including snowmelt, rainfall, and dew and negative values due to soil-surface evaporation.

Figure 4 shows how the surface water fluxes modelled by NoahMP are transferred to CATHY in the coupling mode. During a snow-covered season, surface evaporation, q_{eva}, occurs on the snow surface, consisting of sublimation from ice surface and evaporation from liquid water held by snow ice (Figure 4(e)), and not on the soil surface; thus, it does not affect q_{in} (Figure 4(c)). Water incident on the soil surface, q_{in}, is mainly from snowmelt water (Figure 4(c)), and the discharge at the catchment outlet increases and reaches its peak value (Figure 4(b)) in response to snowmelt. Evaporation from the soil surface starts to increase (Figure 4 (e)), following the elevated soil moisture in response to snowmelt, and then transpiration (q_{root}) increases in later stages following plant growth (Figure 4(d)).

In general, all three experiments (NoahMP, CATHY/NoahMP at 30-m resolution, and CATHY/NoahMP at 90-m resolution) adequately simulated the major peaks and recessions of the daily observed discharges in response to snowmelt (Figure 5). However, evaluated with the Nash–Sutcliffe model efficiency (ε) and root mean square error (RMSE), the CATHY/NoahMP simulations at both 90 and 30-m resolution result in a higher ε and a smaller RMSE than the 1D NoahMP simulation. At 30-m resolution, the CATHY/NoahMP simulation results in a slightly lower ε and a greater RMSE than at 90-m resolution, because of the model not being specifically calibrated for the 30-m simulation (the optimized parameters from the 90-m simulation were used for the 30-m runs). The 3D coupled model improves the simulation during the earlier phase of snowmelt, most readily apparent in the springs of 1970 and 1971 (see also Figure 4 (b)). This may be mainly due to an intrinsic problem of the TOPMODEL-based runoff scheme in 1D NoahMP. The scheme accounts for saturation-excess runoff and relates runoff to surface-saturated area that is controlled by the depth to water table but does not account for perched water tables. In the spring, the rise of the water table may take much longer to reach the ground surface, and thus, runoff generation is delayed, although 1D NoahMP does not include an explicit surface water routing scheme and thus discounts the time for the water to travel from upper reaches to the outlet. Therefore, optimizing only one parameter (the decay factor) may not improve the simulation during all runoff periods; optimizing other parameters in NoahMP such as K_s and the soil texture parameter (or Clapp–Hornberger b parameter) may further improve the simulation. However, to thoroughly assess the model's improvement, optimization of all critical parameters over the whole parameter space and assessment of the probability distribution of the model's performance are necessary (Gulden *et al.*, 2008).

The surface-saturated fraction (F_{sat}) is very important for controlling surface runoff generation and surface evaporation in climate models. It is parameterized in NoahMP as a simple exponential function of the water table depth (see Niu *et al.*, 2011 for details). It has been rarely validated, owing to a dearth of adequate observational data, except for the work of Guntner *et al.* (2004). One-dimensional NoahMP produced

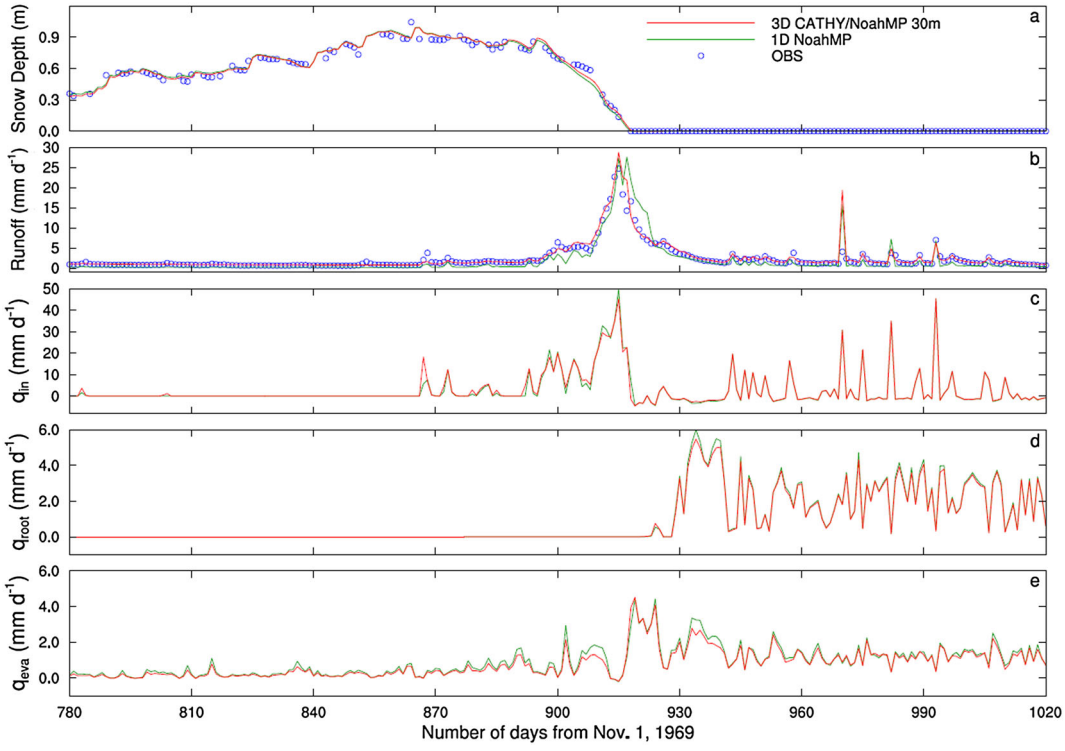

Figure 4. Modelled daily mean (a) snow depth (m), (b) discharge (mm d^{-1}), (c) q_{in} (mm d^{-1}), (d) q_{root} (mm d^{-1}), and (e) q_{eva} (mm d^{-1}) averaged over the subcatchment from the winter snow season of 1971 to the fall of 1972. The observed snow depth and discharge are also included in (a) and (b), respectively.

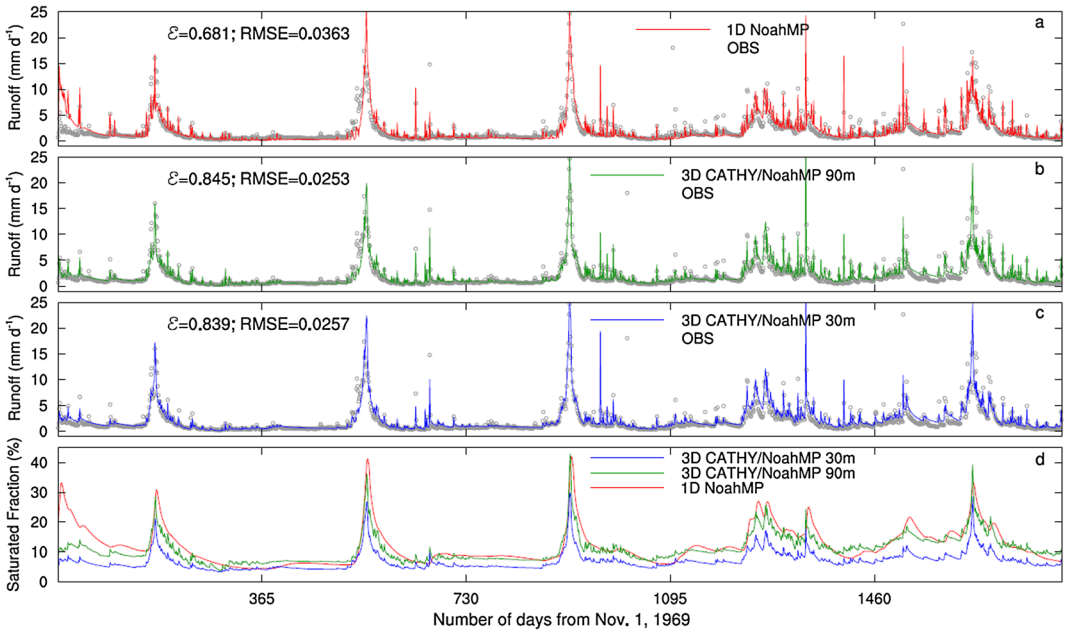

Figure 5. Daily mean discharges (mm d^{-1}) by (a) 1D NoahMP, (b) 3D coupled CATHY/NoahMP at 90-m resolution, and (c) 3D coupled CATHY/NoahMP at 30-m resolution, together with (d) daily mean fractional saturated surface of the W3 subcatchment of the Sleepers River watershed, Vermont. The observed discharge at the outlet of the W3 catchment is also included in (a), (b), and (c). Also shown are the Nash–Sutcliffe model efficiency (ε) and the root mean square error (RMSE) for each simulation.

F_{sat} close to that produced by CATHY/NoahMP at 90-m resolution but systematically greater than that at 30-m resolution by about 3–5% (we believe the 30-m simulation is more realistic). This is consistent with the work of Riley *et al.* (2012), who reported a greater-than-satellite remotely sensed F_{sat} simulated by the NCAR CLM, which uses the same F_{sat} scheme based on TOPMODEL. Such comparisons will be beneficial for revising the TOPMODEL scheme (or optimizing its parameters) used in large-scale hydrological models and in climate models.

CATHY/NoahMP also shows a unique capability of simulating surface-inundated areas and surface water height inferred from surface water pressure, a feature that 1D LSMs do not have. Figure 6 shows the modelled surface water height generated by CATHY/NoahMP at 30 and 90-m resolutions. The simulation at 30-m resolution appears to provide more details in the areas above saturation than the 90-m resolution case. In response to surface water inputs, the modelled surface water height at a lake cell reaches equilibrium (defined as a state wherein the difference of a model variable between two successive spin-up runs is less than 1% of the value of that state variable) faster at 30-m resolution than at 90 m (Figure 6(c)). The modelled surface water height at 30-m resolution varies from 2.5 to 3.0 m in response to seasonal snowmelt. The 90-m resolution simulation shows an increasing trend, implying that the

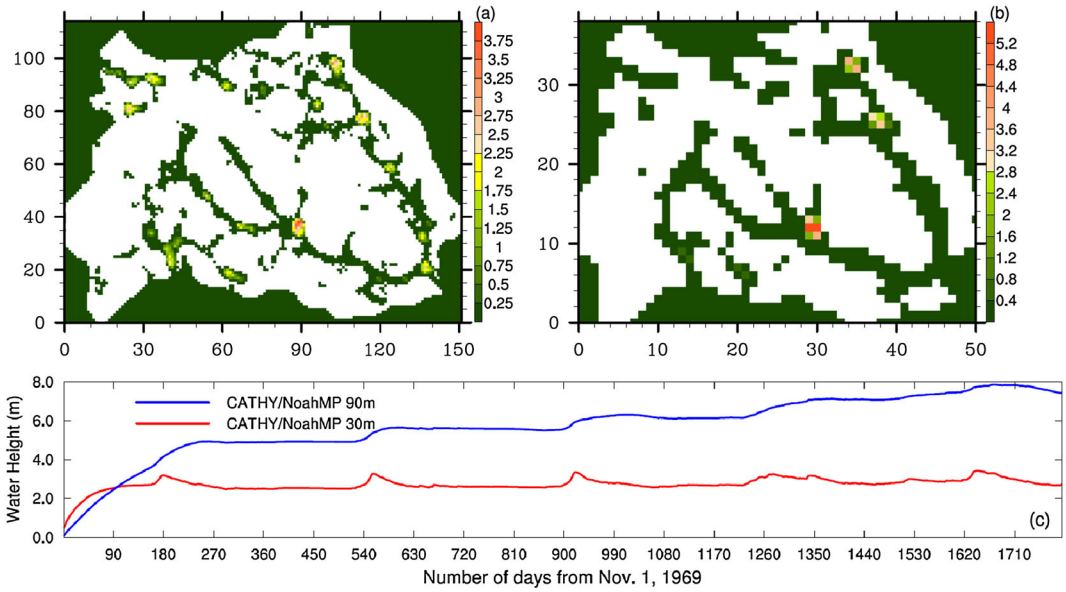

Figure 6. Daily mean surface water height (m) modelled by the coupled CATHY/NoahMP model at (a) 30 and (b) 90-m resolution at day 550, and (c) temporal variation of the daily mean water height of a lake around the grid cell (90, 38) in the 30-m map.

surface water height at this lake cell does not reach an equilibrium state and needs a longer spin-up time, although the total surface water height over the entire catchment does approach an equilibrium state (results not shown). The large difference shown in Figure 6(c) indicates that the modelling results for surface water height are very sensitive to DEM resolution. For lack of observational data at the lake, the model's ability to simulate surface water height cannot be validated in this study. However, the model shows a capability of predicting flash floods and the extent of inundated areas in response to storm events, as well as the variability of the surface water height in lakes in response to seasonal climatic forcings.

The catchment-averaged soil moisture in the upper four soil layers simulated by CATHY/NoahMP at 30 and 90-m resolution shows very little difference (Figure 7). One-dimensional NoahMP produced apparently lower soil moisture for the topmost two layers and slightly lower soil moisture for the bottom two layers. In our earlier simulations, CATHY/NoahMP produced much wetter soil at the bottom layer when it was set up with a zero-flux condition at 2.0 m, as this configuration led to unrealistically shallow water tables. When the zero-flux bottom boundary condition is extended to 4.0 m to better capture the water table dynamics, the soil moisture is also presumed to be more realistically simulated. The 1D NoahMP model produced lower soil moisture in the topmost two layers with a greater amplitude of variation compared with the 3D model, especially during the soil moisture recession period, because of the greater buffering effect and storage capacity available in the 3D coupled model configuration. Previous model intercomparison studies have shown that various 1D LSMs produced a wide range of soil moisture, indicating that accurate modelling of this state variable is a difficult task (Boone *et al.*, 2004). The ability of the 3D coupled model to simulate soil moisture variations in space and time is subject to future studies, as spatially distributed soil property and moisture observations become more readily available.

SUMMARY

In this paper, we have developed a fully integrated model coupling surface–subsurface hydrological flow (CATHY) and land surface–atmosphere ecohydrological processes (NoahMP). We document the major features of both models and the coupling processes in space and time. CATHY describes 3D subsurface flow in variably saturated porous media and surface routing over hillslopes and in streams, whereas NoahMP features multiple parameterization schemes to account for surface energy, water, and carbon fluxes exchanged between various land surfaces and the atmosphere. NoahMP also includes a plant physiology and phenology model describing leaf photosynthesis, respiration, allocation of assimilated carbon to various parts of plant, turnover, and death due to drought and cold stresses. CATHY and NoahMP are coupled by exchanging their fluxes and state variables. CATHY transfers its 3D soil moisture solved at nodes (i.e. intersection points) to NoahMP's grid cells, and NoahMP, in turn, transfers its water fluxes, including snowmelt, surface evaporation, and transpiration, to CATHY's nodes. The resulting model provides a basis for assessing the impacts of climate change on catchment-scale hydrological and ecological dynamics as well as a research tool for investigating, within a single model framework, the influence of different processes and parameterization schemes on the model's performance.

The coupled CATHY/NoahMP model was tested against observations over the energy-limited W3 catchment (8.4 km^2) of the Sleepers River watershed, Vermont. The coupled model, with minor calibration, performs well in simulating SWE, snow depth, and discharges at both 30 and 90-m

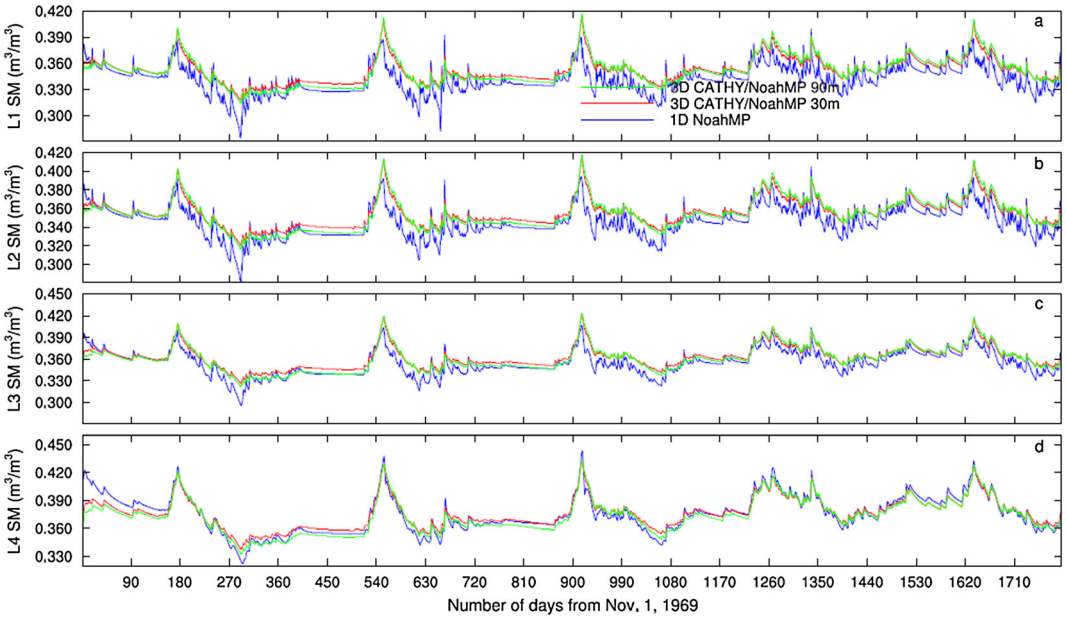

Figure 7. Modelled daily mean soil moisture ($m^3\ m^{-3}$) at four depths: 0.1 (a), 0.4 (b), 1.0 (c), and 2.0 m (d) averaged over the W3 subcatchment of the Sleepers River watershed, Vermont.

surface grid resolutions, with Nash–Sutcliffe model efficiency of the daily discharge being above 0.82. At a coarser resolution (90 m), CATHY/NoahMP results in a slightly better model performance than at a finer resolution (30 m) because of more elaborate calibration at the coarser resolution. Because of computational cost, a thorough calibration of the model at the finer resolution, which may further improve the model's performance, was not conducted in this study. The 3D coupled model improves the simulation of discharge more apparently during the earlier phase of snowmelt in the spring over the 1D model due mainly to an intrinsic problem of the TOPMODEL-based runoff scheme in the 1D NoahMP. Although the 1D NoahMP does not include an explicit surface water routing scheme and thus saves the time for the water to travel from upper reaches to the outlet, the TOPMODEL scheme, which relates runoff to the water table depth generates delayed runoff due to the slow response of water table to snowmelt. Calibration of a single parameter in the 1D model is not adequate, as a thorough assessment would require optimization over the entire parameter space (Gulden *et al*., 2008).

Surface-saturated area is important for parameterizing saturation-excess runoff and biogeochemical processes in large-scale LSMs. The TOPMODEL-based scheme as used in the 1D NoahMP overestimates surface-saturated fraction, as concluded also by Riley *et al*. (2012), who reported an overestimated F_{sat} by the NCAR CLM compared with satellite data. Compared with the 1D model, the coupled 3D model also shows a unique capability of simulating surface-inundated area and surface water height, providing a research tool for predicting flash flood in response to storms as well as lake and wetland dynamics in response to climatic forcing. The resulting model provides a basis for assessing the impacts of climate change on catchment-scale hydrological and ecological processes, and the interactions between these processes.

Assessment of the coupled 3D model is largely limited by the availability of observational data for the W3 subcatchment. Although the 3D model is able to simulate snow mass and discharge quite well, its ability to simulate the dynamics of surface-saturated areas and subsurface soil moisture is subject to future studies where spatially distributed soil property and moisture observations are also available. In a companion paper (Niu *et al*., 2012), a detailed assessment of the coupled model to simulate surface energy, water, and carbon fluxes is performed for a water-limited catchment in a semi-arid climate. These two end-member climates (an energy-limited and a water-limited catchment) were selected to test the coupled ecohydrological model over as broad a range of atmosphere–land surface–subsurface interaction conditions as possible.

ACKNOWLEDGEMENTS

This work was mainly supported by Biosphere 2 and partly by DOE (DE-SC0006773) and NSF (EF 1065790). We thank Marc Stieglitz for providing us with the Sleepers River watershed dataset.

REFERENCES

Beven KJ, Kirkby MJ. 1979. A physically based, variable contributing area model of basin hydrology. *Hydrology Science Bulletin* **24**: 43–69.

Bixio AC, Orlandini S, Paniconi C, Putti M. 1999. Coupled surface runoff and subsurface flow model for catchment simulations. In *Modelling of Transport Processes in Soils at Various Scales in Time and Space: International EurAgEng Workshop*, 583–591, Wageningen Pers: The Netherlands.

Boone A, Habets F, Noilhan J, Clark D, Dirmeyer P, Fox S, Gusev Y, Haddeland I, Koster R, Lohmann D, Mahanama S, Mitchell K, Nasonova O, Niu GY, Pitman A, Polcher J, Shmakin AB, Tanaka K, van den Hurk B, Verant S, Verseghy D, Viterbo P, Yang ZL. 2004. The Rhône-aggregation land surface scheme intercomparison project: an overview. *Journal of Climate* **17**: 187–208.

Brooks RH, Corey AT. 1964. Hydraulic properties of porous media. *Hydrol. Pap. 3*, Colo. State Univ.: Fort Collins.

Brutsaert WA. 1982. *Evaporation into the Atmosphere*, Reidel: Dordrecht; 299 pp.

Camporese M, Paniconi C, Putti M, Orlandini S. 2010. Surface-subsurface flow modeling with path-based runoff routing, boundary condition-based coupling, and assimilation of multisource observation data. *Water Resources Research* **46**: W02512, doi:10.1029/2008WR007536.

Caylor KK, Scanlon TM, Rodriguez-Iturbe I. 2004. Feasible optimality of vegetation patterns in river basins. *Geophysical Research Letters* **31**: L13502, doi:10.1029/2004GL020260.

Chen F, Dudhia J. 2001. Coupling an advanced land surface–hydrology model with the Penn State–NCAR MM5 modeling system. Part I: model implementation and sensitivity. *Monthly Weather Review* **129**: 569–585.

Collatz GJ, Ball JT, Grivet C, Berry JA. 1991. Physiological and environmental regulation of stomatal conductance, photosynthesis and transpiration – a model that includes a laminar boundary layer. *Agricultural and Forest Meteorology* **54**(2–4): 107–136.

Collatz GJ, Ribascarbo M, Berry JA. 1992. A coupled photosynthesis–stomatal conductance model for leaves of C4 plants. *Australian Journal of Plant Physiology* **19**: 519–538.

Deardorff JW. 1978. Efficient prediction of ground surface-temperature and moisture, with inclusion of a layer of vegetation. *Journal of Geophysical Research* **83**: 1889–1903.

Dickinson RE. 1983. Land surface processes and climate-surface albedos and energy balance. In *Theory of Climate, Advances in Geophysics*, Saltzman B (ed). Academic: San Diego, Calif; **25**: 305–353.

Dickinson RE, Shaikh M, Bryant R, Graumlich L. 1998. Interactive canopies for a climate model. *Journal of Climate* **11**: 2823–2836.

Ek MB, Mitchell KE, Lin Y, Rogers E, Grunmann P, Koren V, Gayno G, Tarpley JD. 2003. Implementation of Noah land surface model advancements in the National Centers for Environmental Prediction operational mesoscale Eta model. *Journal of Geophysical Research* **108**(D22): 8851, doi:10.1029/2002JD003296.

Emanuel RE, Epstein HE, McGlynn BL, Welsch DL, Muth DJ, D'Odorico P. 2010. Spatial and temporal controls on watershed ecohydrology in the northern Rocky Mountains. *Water Resources Research* **46**: W11553, doi:10.1029/2009WR008890.

Entekhabi D, Eagleson PS. 1989. Land surface hydrology parameterization for atmospheric general circulation models including subgrid-scale spatial variability. *Journal of Climate* **2**: 816–831.

Famiglietti JS, Wood EF. 1994. Multi-scale modeling of spatially variable water and energy balance processes. *Water Resources Research* **30**(11): 3061–3078.

Fan Y, Miguez-Macho G, Weaver CP, Walko R, Robock A. 2007. Incorporating water table dynamics in climate modeling: 1. Water table observation and equilibrium water table simulations. *Journal of Geophysical Research* **112**: D10125, doi:10.1029/2006JD008111.

Farquhar GD, von Caemmerer S, Berry JA. 1980. A biochemical model of photosynthetic CO_2 assimilation in leaves of C3 species. *Planta* **149**: 78–90.

Gedney N, Cox PM. 2003. The sensitivity of global climate model simulations to the representation of soil moisture heterogeneity. *Journal of Hydrometeorology* **4**: 1265–1675.

van Genuchten MT, Nielsen DR. 1985. On describing and predicting the hydraulic properties of unsaturated soils. *Annals of Geophysics* **3**(5): 615–628.

Gulden LE, Rosero E, Yang ZL, Wagener T, Niu GY. 2008. Model performance, model robustness, and model fitness scores: a new method for identifying good land-surface models. *Geophysics Research Letter* **35**: L11404, doi:10.1029/2008GL033721.

Guntner A, Seibert J, Uhlenbrook S. 2004. Modeling spatial patterns of saturated areas: an evaluation of different terrain indices. *Water Resources Research* **40**: W05114, doi:10.1029/2003WR002864.

Huxman T, Troch PA, Chorover J, Breshears DD, Saleska S, Pelletier J, Zeng X, Espeleta J. 2009. The hills are alive: earth science in a controlled environment, *EOS Transactions, American Geophysical Union* **90**: 120.

Huyakorn PS, Thomas SD, Thompson BM. 1984. Techniques for making finite elements competitive in modeling flow in variably saturated porous media. *Water Resources Research* **20**(8): 1099–1115.

Ivanov VY, Vivoni ER, Bras RL, Entekhabi D. 2004. Catchment hydrologic response with a fully distributed triangulated irregular network model. *Water Resources Research* **40**: W11102, doi:10.1029/2004WR003218.

Kampf SK, Burges SJ. 2007. A framework for classifying and comparing distributed hillslope and catchment hydrologic models. *Water Resources Research* **43**: W05423, doi:10.1029/2006WR005370.

Kollet SJ, Maxwell RM. 2006. Integrated surface–groundwater flow modeling: a free-surface overland flow boundary condition in a parallel groundwater flow model. *Advances in Water Ressources* **29**: 945–958.

Kollet SJ. Maxwell RM. 2008. Capturing the influence of groundwater dynamics on land surface processes using an integrated, distributed watershed model. *Water Resources Research* **44**: W02402, doi:10.1029/2007WR006004.

Koster RD, Suarez MJ, Ducharne A, Stieglitz M, Kumar P. 2000. A catchment-based approach to modeling land surface processes in a general circulation model: 1. Model structure. *Journal of Geophysical Research* **105**(D20): 24,809–24,822.

Liang X, Lettenmaier DP, Wood EF, Burges SJ. 1994. A simple hydrologically based model of land surface water and energy fluxes for general circulation models. *Journal of Geophysical Research* **99**: 14,415– 14,428.

Liang X, Xie Z, Huang M. 2003. A new parameterization for surface and groundwater interactions and its impact on water budgets with the variable infiltration capacity (VIC) land surface model. *Journal of Geophysical Research* **108**(D16): 8613, doi:10.1029/2002JD003090.

Lynch-Stieglitz M. 1994. The development and validation of a simple snow model for GISS GCM. *Journal of Climate* **7**: 1842–1855.

Mackay DS, Band LE. 1998. Extraction and representation of nested catchment areas from digital elevation models in lake-dominated topography. *Water Resources Research* **34**(4): 897–901.

Marks D, Dozier J, Frew J. 1984. Automated basin delineation from digital elevation data. *Geo-processing* **2**: 299–311.

Maxwell RM, Miller NL. 2005. Development of a coupled land surface and groundwater model. *Journal of Hydrometeorology* **6**: 233–247.

Miguez-Macho G, Fan Y, Weaver CP, Walko R, Robock A. 2007. Incorporating water table dynamics in climatevmodeling: 2. Formulation, validation, and soil moisture simulation. *Journal of Geophysical Research* **112**: D13108, doi:10.1029/2006JD008112.

Newman BD, Wilcox BP, Archer SR, Breshears DD, Dahm CN, Duffy CJ, McDowell NG, Phillips FM, Scanlon BR, Vivoni ER. 2006. Ecohydrology of water-limited environments: a scientific vision. *Water Resources Research* **42**: W06302, doi:10.1029/2005WR004141.

Niu GY, Yang ZL. 2004. The effects of canopy processes on snow surface energy and mass balances. *Journal of Geophysical Research* **109**: D23111, doi:10.1029/2004JD004884.

Niu GY, Yang ZL. 2006. Effects of frozen soil on snowmelt runoff and soil water storage at a continental scale. *Journal of Hydrometeorology* **7**(5): 937–952.

Niu GY, Troch PA, Paniconi C, Scott RL, Zeng X, Durcik M, Huxman T, Goodrich D, Pelletier J. 2012. An integrated modeling framework of catchment-scale ecohydrological processes: 2. The role of water subsidy by overland flow on vegetation dynamics. (submitted to *Ecohydrology*).

Niu GY, Yang ZL, Dickinson RE, Gulden LE. 2005. A simple TOPMODEL-based runoff parameterization (SIMTOP) for use in global climate models. *Journal of Geophysical Research* **110**: D21106, doi:10.1029/2005JD006111.

Niu GY, Yang ZL, Dickinson RE, Gulden LE, Su H. 2007. Development of a simple groundwater model for use in climate models and evaluation with Gravity Recovery and Climate Experiment data. *Journal of Geophysical Research* **112**: D07103, doi:10.1029/2006JD007522.

Niu GY, Yang ZL, Mitchell KE, Chen F, Ek MB, Barlage M, Kumar A, Manning K, Niyogi D, Rosero E, Tewari M, Xia YL. 2011. The community Noah land surface model with multiparameterization options (Noah-MP): 1. Model description and evaluation with local-scale measurements. *Journal of Geophysical Research* **116**: D12109, doi:10.1029/2010JD015139.

O'Callaghan JF, Mark DM. 1984. The extraction of drainage networks from digital elevation data. *Computer Vision, Graphics, and Image Processing* **28**: 323–344.

Oleson KW, Lawrence DM, Bonan GB, Flanner MG, Kluzek E, Lawrence PJ, Levis S, Swenson SC, PThornton PE, Dai A, Decker M, Dickinson R, Feddema J, Heald CL, Hoffman F, Lamarque JF, Mahowald N, Niu GY, Qian T, Randerson J, Running S, Sakaguchi K, Slater A, Stöckli R, Wang A, Yang ZL, Zeng X, Zeng X. 2010. Technical Description of version 4.0 of the Community Land Model (CLM), NCAR Technical Note *NCAR/TN-478 + STR*, National Center for Atmospheric Research, Boulder, Colorado, 266 pp. (available at http://www.ccsm.ucar.edu/models/ccsm4.0/clm/CLM4_Tech_Note.pdf).

Orlandini S. 2002. On the spatial variation of resistance to flow in upland channel networks. *Water Resources Research* **38**(10): 1197, doi:10.1029/2001WR001187.

Orlandini S, Moretti G. 2009a. Determination of surface flow paths from gridded elevation data. *Water Resources Research* **45**: W03417, doi:10.1029/2008WR007099.

Orlandini S, Moretti G. 2009b. Comment on "Global search algorithm for nondispersive flow path extraction" by Kyungrock Paik. *Journal of Geophysical Research* **114**: F04004, doi:10.1029/2008JF001193.

Orlandini S, Rosso R. 1996. Diffusion wave modeling of distributed catchment dynamics. *Journal of Hydrological Engineering* **1**(3): 103–113.

Orlandini S, Rosso R. 1998. Parameterization of stream channel geometry in the distributed modeling of catchment dynamics. *Water Resources Research* **34**(8): 1971–1985.

Paniconi C, Putti M. 1994. A comparison of Picard and Newton iteration in the numerical solution of multidimensional variably saturated flow problems. *Water Resources Research* **30**(12): 3357–3374.

Paniconi C, Wood EF. 1993. A detailed model for simulation of catchment scale subsurface hydrologic processes. *Water Resources Research* **29**(6): 1601–1620.

Peters-Lidard CD, Houser PR, Tian Y, Kumar SV, Geiger J, Olden S, Lighty L, Doty B, Dirmeyer P, Adams J, Mitchell K, Wood EF, Sheffield J. 2007. High-performance Earth system modeling with NASA/GSFC's Land Information System. *Innovations in Systems and Software Engineering* **3**(3): 157–165. DOI:10.1007/s11334-007-0028-x

Rigon R, Bertoldi G, Over TM. 2006. GEOtop: a distributed hydrological model with coupled water and energy budgets. *Journal of Hydrometeorology* **7**(3): 371–388.

Riley WJ, Subin ZM, Lawrence DM, Swenson SC, Torn MS, Meng L, Mahowald NM, Hess P. 2012. Barriers to predicting changes in global terrestrial methane fluxes: analyses using CLM4Me, a methane biogeochemistry model integrated in CESM. *Biogeosciences* **8**: 1925–1953.

Riveros-Iregui DA, McGlynn BL, Marshall LA, Welsch DL, Emanuel RE, Epstein HE. 2011. A watershed scale assessment of a process soil CO_2 production and efflux model. *Water Resources Research* **47**: W00J04, doi:10.1029/2010WR009941.

Schaake JC, Koren VI, Duan QY, Mitchell KE, Chen F. 1996. Simple water balance model for estimating runoff at different spatial and temporal scales. *Journal of Geophysical Research* **101**: 7461–7475.

Sellers PJ, Heiser MD, Hall FG. 1992. Relations between surface conductance and spectral vegetation indices at intermediate (100 m^2 to 15 km^2) length scales. *Journal of Geophysical Research* **97**(D17): 19,033–19,059.

Seuffert G, Gross P, Simmer C. 2002. The influence of hydrologic modeling on the predicted local weather: two-way coupling of a mesoscale weather prediction model and a land surface hydrologic model. *Journal of Hydrometeorology* **3**: 505–523.

Shen CP, Phanikumar MS. 2010. A process-based, distributed hydrologic model based on a large-scale method for surface–subsurface coupling. *Advances in Water Resources* **33**: 1524–1541.

Sivapalan M, Beven K, Wood EF. 1987. On hydrologic similarity: 2. A scaled model of storm runoff production. *Water Resources Research* **23**: 2266–2278.

Sulis M, Meyerhoff SB, Paniconi C, Maxwell RM, Putti M, Kollet SJ. 2010. A comparison of two physics-based numerical models for simulating surface water–groundwater interactions. *Advances in Water Resources* **33**: 456–467, doi:10.1016/j.advwatres.2010.01.010.

Tarboton DG. 1997. A new method for the determination of flow directions and contributing areas in grid digital elevation models. *Water Resources Research* **33**(2): 309–319.

Thompson SE, Harman CJ, Troch PA, Brooks PD, Sivapalan M. 2011. Spatial scale dependence of ecohydrologically mediated water balance partitioning: a synthesis framework for catchment ecohydrology. *Water Resources Research* **47**: W00J03, doi:10.1029/2010WR009998.

Weill S, Mazzia A, Putti M, Paniconi C. 2011. Coupling water flow and solute transport into a physically-based surface–subsurface hydrological model. *Advances in Water Resources* **34**: 128–136, doi:10.1016/j.advwatres.2010.10.001.

Xia Y, Mitchell K, Ek M, Cosgrove B, Sheffield J, Luo L, Alonge C, Wei H, Meng J, Livneh B, Duan Q, Lohmann D. 2012. Continental-scale water and energy flux analysis and validation for the North American Land Data Assimilation System project phase 2 (NLDAS-2): 1. Intercomparison and application of model products. *Journal of Geophysical Research* **117**: D03109, doi:10.1029/2011JD016048.

Xie ZH, Di ZH, Luo ZD, Ma Q. 2012. A quasi-three-dimensional variably saturated groundwater flow model for climate modeling. *Journal of Hydrometeorology* **13**: 27–46.

Yang ZL, Niu GY. 2003. The versatile integrator of surface and atmosphere processes (VISA) part I: model description. *Global Planet Change* **38**: 175–189.

Yeh PJF, Eltahir EAB. 2005. Representation of water table dynamics in a land surface scheme. Part I: model development. *Journal of Climate* **18**: 1861–1880.

York JP, Person M, Gutowski WJ, Winter TC. 2002. Putting aquifers into atmospheric simulation models: An example from the Mill Creek Watershed, northeastern Kansas. *Advances in Water Resources* **25**(2): 221–238.

Yu ZB, Pollard D, Cheng L. 2006. On continental-scale hydrologic simulations with a coupled hydrologic model. *Journal of Hydrology* **331**: 110–124.

Zeng XD, Zeng X, Barlage M. 2008. Growing temperate shrubs over arid and semiarid regions in the NCAR Dynamic Global Vegetation Model (CLM-DGVM). *Global Biogeochemical Cycles* **22**: GB3003, doi: 10.1029/2007 GB003014.